Bound states and transmission antiresonances in parabolically confined cross structures: Influence of weak magnetic fields

R. Akis
Center for Solid State Electronics Research, Center for Systems Science and Engineering, and Department of Electrical Engineering, Arizona State University, Tempe, Arizona 85287

P. Vasilopoulos
Department of Physics, Concordia University, 1455 de Maisonneuve Boulevard O, Montréal, Québec, Canada, H3G 1M8

P. Debray
Service de Physique de l'Etat Condense and Centre National del la Recherche Scientific, Centre d'Etudes de Saclay, 91191 Gif-sur-Yvette, France

(Received 7 April 1997)

The ballistic conductance through a device consisting of quantum wires, to which two stubs are attached laterally, is calculated assuming parabolic confining potentials of frequencies ω_w for the wires and ω_s for the stubs. As a function of the ratio ω_w/ω_s the conductance shows nearly periodic minima associated with quasibound states forming in the stubbed region. Applying a magnetic field B normal to the plane of the device changes the symmetry of the wave functions with respect to the center of the wires and leads to *new* quasibound states in the stubs. The presence of the magnetic field can also lead to a second kind of state, trapped mainly in the wires by the corners of the confining potentials, that yields conductance minima as well. In either case, these bound states form for *weak B* and strong confining frequencies and thus are *not* edge states. Finally, we show experimental evidence for the presence of these quasibound states. [S0163-1829(97)03639-4]

I. INTRODUCTION

Technological advances in microfabrication techniques now allow the manufacture of semiconductor structures that have dimensions smaller than the elastic and inelastic mean scattering lengths. In such *mesoscopic* structures, the electronic transport is *ballistic*,[1] and the conductance is governed by the fact that the electrons behave like quantum mechanical waves. This is particularly true at low temperatures.

The wavelike behavior of electrons in such structures has led to the study of devices that are analogous to those used in microwave technology. The simplest such device is the quantum wire (QW), which can be thought of as an electronic waveguide. Some more complicated structures involve having QW's cross to form junctions, attaching finite branches to the QW's so that they become corrugated, and connecting the QW's to the electronic equivalent of a resonant cavity. These closely related structures have generated experimental and theoretical interest.[2–9] In particular, resonant tunneling and quasibound states in stub and cross structures have been focused on because in these systems the electrons are not bound classically by any potential barriers. In addition, they are unusual in that the presence of quasibound states can lead to resonant *reflection* instead of transmission, i.e., transmission *antiresonances*.

A special type of structure in this class is the electron stub tuner (EST), in which the length of the stub, laterally attached to the QW, would be controlled by an independent gate. If the width of the QW and the stub are such that both allow only a single propagating mode for a given incident energy, then the conductance G is a periodic function of the stub length c, with G oscillating between 0 and 1, in units of $2e^2/h$, making it potentially useful as a type of transistor.[10] The conductance minima that result can be attributed to *destructive* interference between the electron waves in the wire and those reflected from the stub. A more sophisticated device is the double electron stub tuner (DEST) depicted in Fig. 1(a). If the length of the DEST is kept *fixed* while it is being made asymmetric by suitably synchronized gate voltages, a conductance output, nearly square wave in form, can be achieved as a function of the degree of asymmetry with potential uses in analog-to-digital converters.[11]

In this paper we consider a few important issues with regard to these devices. First of all, in previous theoretical work on cavity and stub structures, the confining potentials were always assumed to be infinite square well in nature.[2–12] However, it is well known that for very narrow QW's a parabolic potential is more appropriate.[13] In such a case the width of the electronic wave functions and thus the device dimensions *are not well defined*. After briefly presenting the formalism in Sec. II, we will present *the zero field results* for a DEST, which show a nearly periodic conductance as a function of the ratio ω_w/ω_s even under these circumstances. Some of these results are compared with those obtained assuming a square confinement.

Second, ''true'' EST's and DEST's, with independent gates controlling the stub lengths, have yet to be fabricated. Thus far, experiments have only been done on cavity structures in which the conductance was studied as a function of a gate voltage V_g that affected several of the device dimensions simultaneously, making it difficult to interpret the results definitively as resulting from the interference effects mentioned above. However, G has been measured in these structures as a function of a *weak* perpendicular magnetic

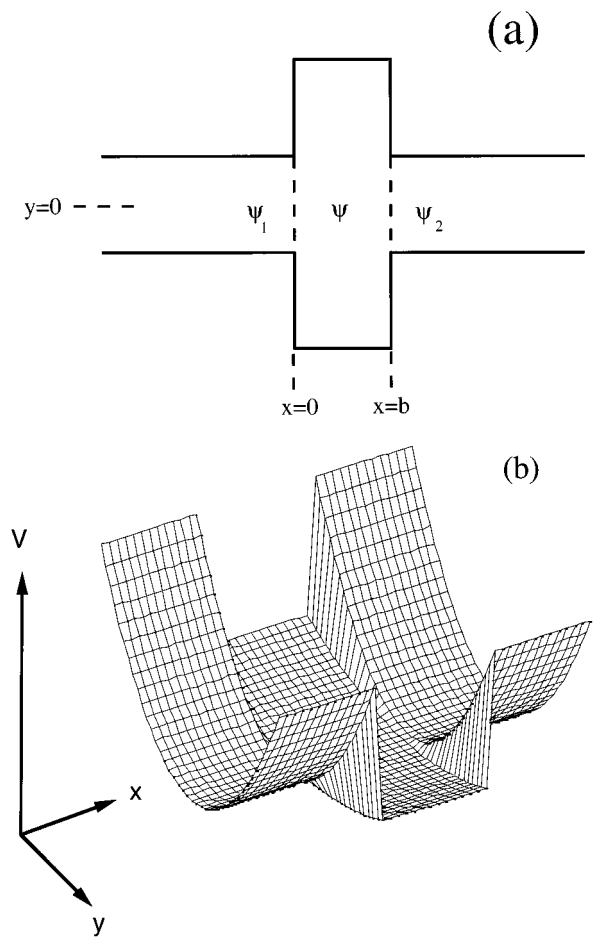

FIG. 1. (a) A stubbed cavity of width b connected to two quantum wires. (b) The confining potential in the wires and the stubbed cavity. The picture is generated with $\hbar\omega_w = 6.39$ meV, $\hbar\omega_s = 2.8$ meV, and $b = 300$ Å. The x range is from -300 Å to 600 Å and the y range from -800 Å to 800 Å.

field B as well for fixed V_g.[14] The results show minima in G as a function of B. The values of B and the confining frequencies are such that edge states do not occur and so much of the previous work on quantum dots is not applicable. As we shall show in Sec. III, such minima can arise in DEST's when electrons are reflected resonantly from quasibound states in the stubs. We further show that *new* quasibound states are created when $B \neq 0$ that are not present in zero field. This happens because B changes the symmetry of the wave functions at zero field with respect to the transverse direction y and leads to *new* couplings between the wire and stub wave functions. In Sec. IV, we show results for actual experiments and interpret them qualitatively in terms of those of Sec. III. Conclusions follow in Sec. V.

II. FORMULATION OF THE TRANSMISSION PROBLEM

In this paper we consider parabolic confinement in the presence of a perpendicular magnetic field $\mathbf{B} = (0,0,B)$. For parabolic confinement along the y axis in the wire (w) and stub (s) regions, we use a potential of the form

$$V_{w,s}(y) = m^* \omega_{w,s}^2 y^2/2, \tag{1}$$

where m^* is the effective electron mass. The confining potential for a model DEST is depicted three dimensionally in Fig. 1(b). The narrower parabolas, defined by the frequency ω_w, represent the two parts of the QW; the wider parabola, defined by $\omega_s < \omega_w$, represents the stubbed region. The confinement in the stubs along x is achieved essentially through the difference in stub and wire potentials, $\Delta V(y) = V_w(y) - V_s(y)$, so that only a *finite* potential barrier is created. As a result, the electronic wave function in the stub regions will not go to zero at the boundaries and thus it can spill over into the QW. This is a feature our present model shares with saddle potentials that is absent in infinite square-well models used in past calculations.

To evaluate the transmission through the device depicted in Fig. 1, we solve Schrödinger's equation on a mesh, using an iterative matrix method. We summarize the essentials of the method below and refer to Ref. 15 for all the mathematical details. The general situation is one in which the QW's, which are connected to the stub structure, extend outward to $\pm\infty$ along the x direction. The problem is solved on a square lattice of constant a. Along the y direction, the system must be cutoff after a finite number of lattice sites, say M. Thus, the situation is one in which the parabolic QW's that are depicted are in fact enclosed within a larger waveguide that is bounded by infinite potential barriers. The region of interest, containing the actual stub structure, can be broken down into a series of slices along the x direction. The discrete form of the Hamiltonian relates quantum mechanical amplitudes between adjacent slices. Using a finite difference approximation and keeping only terms up to first order in the derivative, this has the form

$$(E_F - \mathbf{H}_j)\psi_j + \mathbf{H}_{j,j+1}\psi_{j-1} + \mathbf{H}_{j,j-1}\psi_{j+1} = 0, \tag{2}$$

where ψ_j is a M-dimensional column vector containing the amplitudes of the jth strip. The matrices $\mathbf{H}_j$ represent the Hamiltonians for the individual slices.

When the derivatives are replaced by finite differences, the kinetic energy terms of the Hamiltonian get mapped onto a tight-binding model with $t = -\hbar^2/2m^*a^2$ representing the nearest-neighbor hopping. To include the effects of the confining potential, one adds to the on-site energies, which occur along the diagonals of $\mathbf{H}_j$, the terms $v_{j,m}$, which represent the potential on site (j,m) in units of t. Parabolic confinement can be modeled easily using Eq. (1) for $v(l,m)$, with $y = a[m - (M+1/2)]$, so that $y = 0$ occurs at the center of each slice. The matrices $\mathbf{H}_{j,j+1}$ and $\mathbf{H}_{j,j-1}$ give the interstrip coupling and are related by $\mathbf{H}_{j,j+1} = \mathbf{H}_{j,j-1}^*$. We use the gauge $\mathbf{A} = (-By,0,0)$, which ensures that the magnetic field points along the z direction. In this gauge, these matrices have only diagonal elements and are given by $\mathbf{H}_{j,j+1}(l,l) = -t\exp(2\pi i\beta l)$, where $\beta = Ba^2/\phi_0$ is the magnetic flux per unit cell and $\phi_0 = \hbar/e$. Equation (2) can be used to derive a transfer matrix which allows us to translate across the system and thus calculate the transmission coefficients which enter the Landauer-Büttiker formula for the conductance. Transfer matrices however are notoriously unstable due to exponentially growing and decaying evanescent modes. This problem was overcome in Ref. 15 by performing some clever matrix manipulations and turning the process of translating across the system into an iterative proce-

dure involving a series of scattering matrices, rather than simply multiplying transfer matrices together. It has been found that the method gives results equivalent to those of the recursive Green's function technique,[15] which is the most common approach to this type of problem. Its advantage over the latter is that it is conceptually simpler and one can quite easily reconstruct the wave function. Once the procedure is complete, one obtains the transmission coefficients, t_{nm}, and reflection coefficients, r_{nm}, for the individual modes. Given these, the amplitudes of the wave functions at specific values of x and y can be obtained by a progressive backward substitution.

The total transmission T is given by

$$T=\sum_{nm} T_{nm}=\sum_{nm} |t_{nm}|^2 \frac{v_n}{v_m}, \tag{3}$$

where v_n and v_m correspond to the velocities of the transmitted and incident modes, respectively, and the sum is over *propagating* channels only. The conductance G then at zero temperature is given by the Landauer-Büttiker formula: $G=(2e^2/h)T$.

As mentioned above, Eq. (2) essentially corresponds to a tight-binding model. As such, the energy dispersion relation with respect to wave vector k is of the form of cosine rather than being parabolic, which is what is expected for the continuous case. However, if E_F is such that one is near the bottom of the tight-binding energy band, then we have $\cos(k)\sim k^2$, and the tight-binding model then becomes a good representation of the continuous model. To ensure this, the lattice spacing a should be much smaller than the Fermi wavelength λ_F ($a \ll \lambda_F$). For the calculations described in the subsequent sections, we used typically $E_F=9$ meV, which corresponds to $\lambda_F \sim 500$ Å, and $a=40$ Å, so that λ_F/a was always larger than 10. This is good enough typically to get a good match with the continuous model. To verify this, the results shown in the next section for zero field were compared with those obtained using a mode-matching technique.[12] We found that the conductance traces generated by the two methods were virtually indistinguishable. In zero field, mode-matching techniques are the method of choice since then the modes can be expressed as analytical expressions and the mathematics is relatively simple. However, in finite field, the situation is much more complicated and the modes generally have to be determined numerically. In that case, using a lattice technique such as that employed here gives the maximum amount of flexibility in solving the problem.

Since we do work in the regime of small a, it will be convenient to make reference to the modes that occur in the continuous case. The nth channel wave number α_n in the wire is

$$\alpha_n=\frac{\Omega_w}{\omega_w}\sqrt{\frac{2m^*}{\hbar^2}[E_F-(n+1/2)\hbar\Omega_w]}. \tag{4}$$

Similarly, in the stub region, the wave number γ_m takes the form

$$\gamma_m=\frac{\Omega_s}{\omega_s}\sqrt{\frac{2m^*}{\hbar^2}[E_F-(m+1/2)\hbar\Omega_s]}. \tag{5}$$

Here $\Omega_{s,w}^2=\omega_{s,w}^2+\omega_c^2$ and $\omega_c=|e|B/m^*$ is the cyclotron frequency. The *modes* ϕ_n along the y axis depend on whether the waves are traveling in the positive $e^{i\alpha_n x}$ or negative ($e^{-i\alpha_n x}$) x direction. We thus have wire modes, $\phi_n^{w\pm}(y)=\varphi_n^w[y\mp(\hbar\omega_c/m^*\Omega_w^2)\alpha_n]$, and stub modes, $\phi_m^{s\pm}(y)=\varphi_m^s(y\mp(\hbar\omega_c/m^*\Omega_s^2)\gamma_m)$, where $\varphi_j^\omega(y)$ is the jth harmonic oscillator (HO) wave function. Notice that for $B=0$, we have $\varphi^+(y)=\varphi^-(y)$. It should be noted that generally the number of propagating modes is dwarfed by the number of evanescent modes. In our discrete model, for a given direction, the *total* number of modes (propagating and evanescent) in the calculation is M, the number of lattice sites along the y axis defined earlier. We have used $M=91$ typically, so that we usually have about ~ 90 evanescent modes involved in the calculation. In the continuous case, the number of evanescent modes is of course infinite, but it has been found in mode-matching calculations[12] that only say ~ 5 evanescent modes need to be included to get converging results for a problem that involves one propagating mode.

III. RESULTS

A. Zero field

In previous theoretical work on EST's, with stub length c and width b, a periodic conductance output has been obtained, as a function of c, for infinite square-well confinement; the period δc is given by

$$\delta c=\pi/\sqrt{2m^*E_F/\hbar^2-(\pi/b)^2}=\lambda_s/2, \tag{6}$$

when only one mode is allowed in the QW and stub regions. Equation (6) is a restatement of the condition for *destructive* interference, $k_s\delta c=\pi$, since $\lambda_s=2\pi/k_s$ is the electronic wavelength along the stub. Notice that the period *increases* as b is made smaller. For a *symmetric* DEST,[16] this period is doubled, so that $\delta c=\lambda_s$.

An interesting question is whether or not the conductance remains periodic if the confinement is instead *parabolic*, particularly when considering that in this case the stub length is no longer well defined. In the pertinent literature it is quite common to use the classical turning points to define an *effective* half width $W_{\rm eff}$ of the parabolic well through $E_F=m^*\omega^2W_{\rm eff}^2/2$. Taking $\omega=\omega_s$ gives an effective stub length

$$c_{\rm eff}=2W_{\rm eff}=2\sqrt{\frac{2E_F}{m^*}}\frac{1}{\omega_s}. \tag{7}$$

If the DEST in the parabolic case behaves in a manner similar to that of past calculations, one might expect then that the conductance G of a DEST to be a periodic function of $1/\omega_s$ for fixed E_F. As we show in Fig. 2(a), this is in fact the case. We plot G as a function of ω_w/ω_s for *fixed* $\hbar\omega_w=6.39$ meV and $E_F=9$ meV so that there is one propagating mode in the connecting quantum wires. The width of the stub is $b=400$ Å (solid curve) and $b=350$ Å (dashed curve). When b decreases the period increases; this is consistent with the results for infinite square-well confinement as expressed in Eq. (7).

The transmission minima displayed in Fig. 2(a) can be considered to occur as a result of destructive interference. An

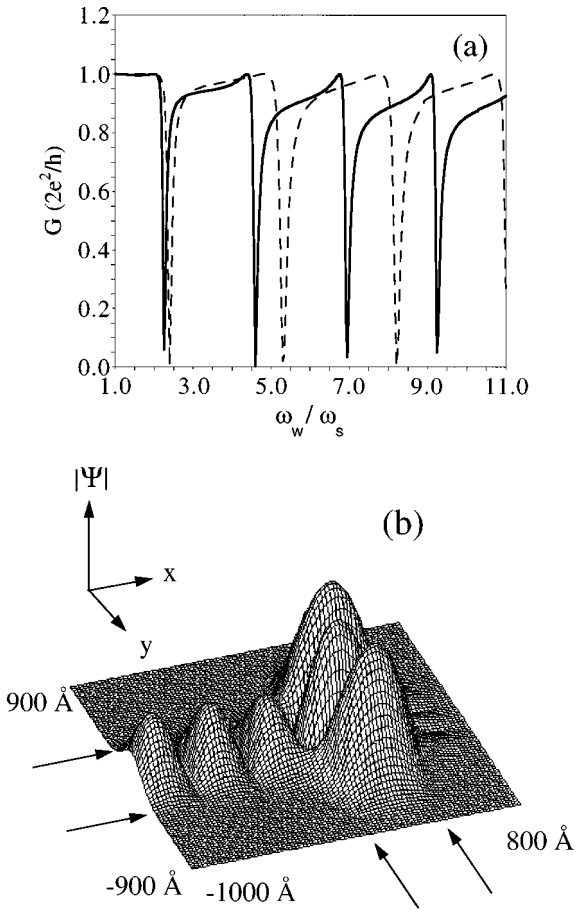

FIG. 2. (a) Conductance G vs ω_w/ω_s for $b=400$ Å (solid line) and $b=350$ Å (dashed) with *fixed* $\omega_w=6.39$ meV and $E=9$ meV. (b) A three-dimensional plot of $|\psi(x,y)|$ vs x and y for $b=400$ Å and $\omega_s=2.88$ meV. This corresponds to the first minimum in the solid curve in (a). The two arrows on the bottom right indicate the edges of the cavity and those on the left the width $W_{\rm eff}$ of the quantum wire.

alternate but complementary point of view is that they occur as a result of resonant *reflection* from quasibound states in the stubbed cavity. They are transmission *antiresonances*. This is illustrated in Fig. 2(b), where $|\psi(x,y)|$ is plotted as a function of x and y. To generate this plot, we have set $E_F=9$ meV, $b=400$ Å, and set $\hbar\omega_s=2.89$ meV, so that $\omega_w/\omega_s=2.21$. The picture corresponds to the *first* transmission minimum in the solid curve in Fig. 2(a). A standing wave corresponding to a quasibound state is apparent in the cavity region between the arrows along the x axis. This state is somewhat similar in appearance to those obtained for square-well potentials.[8]

Further insight into the antiresonances is obtained as follows. Since only one mode is occupied in the quantum wires, the full wave function $\phi(x,y)$ goes as the $n=0$ HO wave function, $\varphi_0^{\omega_w}(y)$ for a set value of x. What is interesting is that the standing wave in the cavity region, despite being obtained by summing over the contributions of many HO wave functions, can be associated with the $n=2$ HO wave function $\varphi_2^{\omega_s}(y)$. In particular, if we set $x=x_0$, where x_0 represents *the center of the stub* (200 Å in this case), then $\psi(x_0,y)$ can be fit almost perfectly by using $\varphi_2^{\omega_s}(y)$ *alone*. While this is not true away from $x=x_0$, $\psi(x,y)$ in the stub region keeps the basic $n=2$ HO form and thus it remains *even* with respect to $y=0$, the center of the quantum wires. Consequently, the conductance minima or antiresonances can be attributed to an *even-even* coupling between the $n=0$ state in the wire and the $n=2$ state bound in the stubbed cavity or DEST. The other minima in the solid curve of Fig. 2 can similarly be associated with an even-even coupling between the $n=0$ and $n=4,6$, etc., states. Coupling between the even, in the wire, and odd, in the stub, HO states does not occur because they are orthogonal to each other.

So far the results are similar to those obtained for a square-well confinement and standing wave patterns analogous to Fig. 2(b) have also been obtained.[12,17] The main difference between the two cases is that in the square-well case the evanescent modes *in the connecting QW's* case tend to decay very slowly. Thus, a long exponential ''tail'' is left in the wave function in the exiting QW, even if there is 100% reflection of the incident propagating mode. This would be a major liability in the fabrication of an operating device, since the presence of the ''tail'' may result in resonant tunneling rather than resonant reflection thus making it difficult to manufacture a device that produces the desired effect. No such tail is apparent in the figure. The fast decay of the evanescent modes in the case of a parabolic potential is related to the wave numbers given by Eqs. (4) and (5) rather than by Eq. (6).

B. Finite field

1. Offset or field. We now consider a finite but *weak* magnetic field B. By *weak* we mean a field that is not strong enough to push the wave functions completely over to one side. We are *not* in the edge-state regime. The use of the term ''weak'' is appropriate to the experimental situation described in Sec. IV, where the dimensions of the experimental samples were several hundred to a few thousand Å, which is our motivation. For a QW with a $c_{\rm eff}$ of a few hundred Å, one expects $\omega_c \ll \omega_w$ for $B<1$ T. In addition, this regime has been much less explored than the edge-state regime. For simplicity we neglect the Zeeman splitting.

In Fig. 3(a) we again plot G as a function ω_w/ω_s for fixed $E=9$ meV, $\hbar\omega_w=6.39$ meV and $b=400$ Å, for three different situations, the upper two curves offset by $G=1$ and $G=2$, respectively, for clarity. The bottom curve is the same as the solid curve in Fig. 2(a). For the middle curve, we have put in a small offset, $d=20$ Å, so that the DEST is now *asymmetric*, with potential $V_{\rm DEST}(y)\rightarrow m^*\omega_s^2(y+d)^2/2$. We see that with the asymmetry the antiresonances that occur in the symmetric case are now shifted down slightly. Second, and more importantly, a whole new set of antiresonances occur in between the original minima. These occur due to the the breaking of symmetry of the wave functions, allowing the even $n=0$ QW state to now couple with the odd states ($n=1,3,5,\ldots$) trapped in the DEST. A very similar behavior has been noted in the case of square-well confinement. The upper curve is for a *symmetric* DEST, but now in the presence of a finite magnetic field, $B=0.3$ T. We see that the presence of the magnetic field produces much the same result as the asymmetry—the shifting of the original antiresonances, and the appearance of the new set of minima at vir-

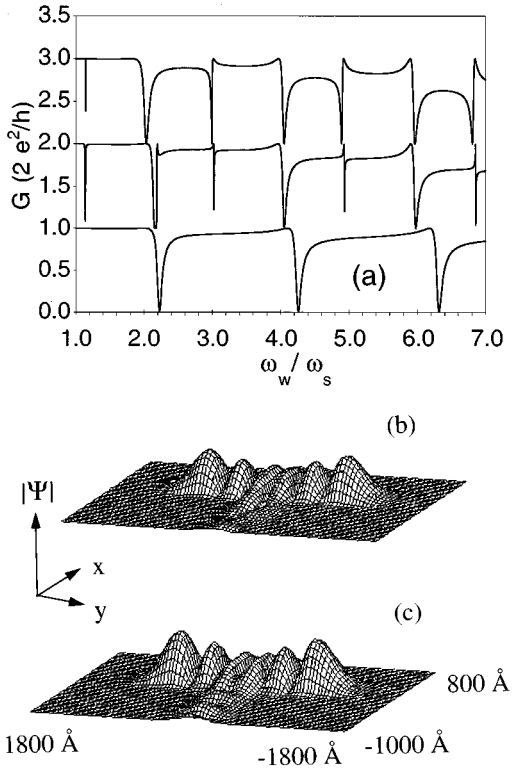

FIG. 3. (a) Conductance G vs ω_w/ω_s for $b=400$ Å, $\omega_w=6.39$ meV, and $E=9$ meV. The bottom curve is for a symmetric DEST at $B=0$ T. For the middle curve, offset by $G=1$, the DEST has been made *asymmetric* by a factor of $d=20$ Å. For the top curve, offset by $G=2$, a $B=0.3$ T has been applied. Notice the additional antiresonances that occur in the presence of finite asymmetry and magnetic field. (b) $|\psi(x,y)|$ vs x and y is plotted for $\omega_w/\omega_s=4.935$ and $d=20$ Å. This quasibound state corresponds to the fifth minimum in the middle curve in (a). (c) As in (b) but for $B=0.3$ T and $\omega_w/\omega_s=4.896$. This state corresponds to the fifth minimum in the top curve in (a).

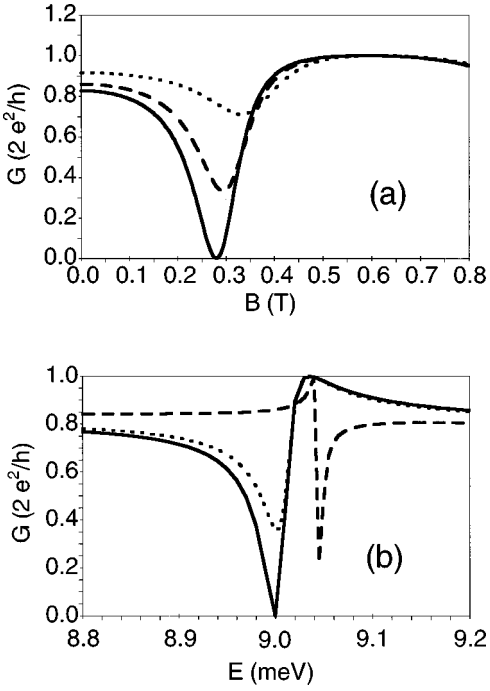

FIG. 4. (a) Conductance G vs B for $b=400$ Å, $\omega_w/\omega_s=4.9$. The solid curve is for a *symmetric* DEST and the dashed and dotted curves for an *asymmetric* one with $d=20$ Å and $d=40$ Å, respectively. (b) Conductance G vs E for $b=400$ Å and $\omega_w/\omega_s=4.9$. The solid curve is for $B=0.28$ T and $d=0$ Å and the dashed one for $B=0$ and $d=20$ Å. The dotted curve is for $B=0.28$ T and $d=20$ Å.

tually the same locations. In Fig. 3(b) we plot $|\psi(x,y)|$ for $\omega_w/\omega_s=4.935$ and $d=20$ Å ($G\sim 0$ for these parameters). Here, the antiresonance wave function has six lobes, indicating the coupling of a $n=5$ odd state in the DEST with the $n=0$ even state in the QW in this case. The corresponding wave function in the presence of a magnetic field is shown in Fig. 3(c) for $\omega_w/\omega_s=4.896$ and $B=0.3$ T. The state shown in this picture is almost indistinguishable from the previous one. Interestingly, the most significant difference between the two pictures occurs in the incident waves. In the finite field case a standing wave appears that is quite similar to the one evident in Fig. 2(b). In the asymmetric case, the waves have a more irregular appearance. One obtains similar results for the other even-odd antiresonances.

Given these results, we conclude the coupling between even and odd states in the presence of a magnetic field occurs here because, when B is finite, *the symmetry about $y=0$ is broken*. Noting that the wave function in Fig. 3(c) appears almost completely symmetric about $y=0$, it is obvious that the presence of edge states is not required for this coupling to take place. In fact, it can occur for arbitrarily small B. However, the smaller B is, the narrower the even-odd antiresonances that occur in Fig. 3(a) become. Another important point is that the position of the antiresonances depends on the value of the magnetic field. For example, the first antiresonance, which corresponds to a $n=0$ QW $-n=1$ DEST coupling, occurs at $\omega_w/\omega_s=1.1164$ for $B=0.11$ T, $\omega_w/\omega_s=1.17$ for $B=0.29$ T, and $\omega_w/\omega_s=1.18$ for $B=0.46$ T. This shifting of the resonance as a function of B for different choices of ω_w/ω_s can be understood, at least in part, in terms of the lining up of the energy level of the bound state of the cavity, E_{bound}, with that of the incident electrons, E_F, which is necessary for a resonance effect to occur. From our previous discussion about fitting the wave function in the DEST, it is apparent that the energy level structure of the quasibound states is tied to Ω_s. A larger (smaller) value of ω_w/ω_s means that ω_s is smaller (larger), thus a larger (smaller) value of B is required to ensure that Ω_s remains at the value that lines up the Fermi level with the bound state level. This argument, however, is somewhat oversimplified in that the bound state energy is not determined by Ω_s alone. The bound states are confined along *both* the x and y directions and so the x confinement must neccessary contribute to the energy of the $n=1$ bound state, so that we should have $E_{\text{bound}}=3\hbar\Omega_s/2+E_x$. However, as the confinement along x is incomplete and the system is open, the contribution E_x is difficult to quantify, at least analytically. Importantly, as B changes Ω_s, the confining potential in the stub along x is also being altered, thus complicating the physical picture. As a result, the value of Ω_s for which antiresonance occurs is slightly different for different values of B. The lining up of QW and DEST energy levels is also the likely explanation of the observed downward shift in both the finite B and finite d cases.

2. Offset and field. In Fig. 4(a) we plot G vs B for fixed

$\omega_w/\omega_s = 4.9$, which corresponds to the $n=0-n=5$ antiresonance. The solid curve corresponds to the DEST being symmetric. The broad minimum at about ~ 0.28 corresponds to the antiresonance in question. It is interesting to see what happens when *a finite B and a finite offset* are present at the same time, as individually they appear to have similar effects. The dashed and dotted curves correspond to $d=20$ Å and $d=40$ Å, respectively. Oddly, the conductance minima become shallower for increased d, as if the magnetic field and asymmetry are canceling each other out. Importantly, essentially the same curves are generated if we replace d with $-d$. A clue to this behavior can be seen in Fig. 3(a). While the antiresonances occur at essentially the same spots, the line shapes are different, with $G=1$ followed by $G=0$ in the case of finite d, and almost exactly the *mirror opposite* for finite B. In either case, the line shapes are asymmetric, that is, they are of *Fano* type. The occurence of Fano antiresonances in stub structures has been the subject of several papers, typically using simple qualitative models[5–7] (stub and wire both treated as being purely one dimensional). Stub structures, unlike say a double barrier problem, yield *both* transmission *poles* in the complex energy plane, the real part of which is associated with the energy of the quasibound states and yield unit transmission, and transmission *zeroes* (the antiresonances). If the pole and the zero do not occur at the same location in energy, one obtains the asymmetric Fano line shape. This gives a $G=1$ peak followed by a $G=0$ minimum when $E_{\text{pole}}<E_{\text{zero}}$, and the opposite when $E_{\text{pole}}>E_{\text{zero}}$. Figure 3(a), however, shows the antiresonances as a function of ω_w/ω_s, which we remind the reader is a measure of stub length for fixed ω_w.

The ''flipping'' of the Fano shaped antiresonance also occurs with respect to *energy* and this is shown in Fig. 4(b), where G vs E is plotted for fixed $\omega_w/\omega_s=4.9$. Once again, the minima here correspond to the $n=0-n=5$ antiresonance. The solid curve corresponds to $B=0.28$ T and $d=0$, while the dashed curve is for $B=0$ and $d=20$ Å. Note that the conductance minima occur at slightly different locations. The dotted curve has both $B=0.28$ T and $d=20$ Å, which shows the hybrid line shape, the result of the ''competition'' between the two sources of symmetry breaking. In the region of the minimum, this third curve looks somewhat like an average between the other two curves. We note that the conductance maximum follows the minimum in the combined curve, like the finite B only curve. We note that the minimum is much wider for the finite B only curve than for the d only curve, indicating that the finite B is producing a stronger effect in comparison to the finite d in this case, and is essentially winning out. Again, referring back to Fig. 3(a), we note that the ''flipping'' effect does not occur when the field B is turned on for the even-even antiresonances, presumably because we consider a relatively weak field B.

3. Two conductance minima. In Fig. 5(a) we again plot G vs B. However, unlike the previous example, *two* transmission minima are apparent for each of the curves shown here. The solid, dashed, and dotted curves correspond to $\omega_w/\omega_s=3.0$, 2.91, and 2.85, respectively. In Fig. 5(b), $|\psi(x,y)|$ is plotted as a function of x and y for the first minimum in the $\omega_w/\omega_s=3.0$ curve, which occurs at $B=0.27$ T. Unlike the previous wave function plots, we are looking directly from above and higher amplitudes are represented by darker shading. The incident electron waves are traveling from the top to the bottom in this picture. The quasibound state in this case has four lobes along the length of the stub and thus represents coupling between $n=0$ and $n=3$ states and is yet another example of the even-odd coupling phenomenon we have already pointed out. More interesting is the wave function that corresponds to the second minimum at $B=0.67$ T, which is plotted in Fig. 5(c). Here the wave function again has four lobes, but in this case there are two each in *both* the x and y directions. The quasibound state shown here does not arise from confinement by the stubs, but is held in place by the corners formed by the intersection points of the stub and wire potentials. Quasibound states of this type were first found to occur theoretically in intersecting quantum wires in a situation analogous to having stubs of infinite length by Schult, Wyld, and Ravenhall.[3] They pointed out two such ''intersection'' states, the lower energy state consisting of one large lobe in the intersection region,

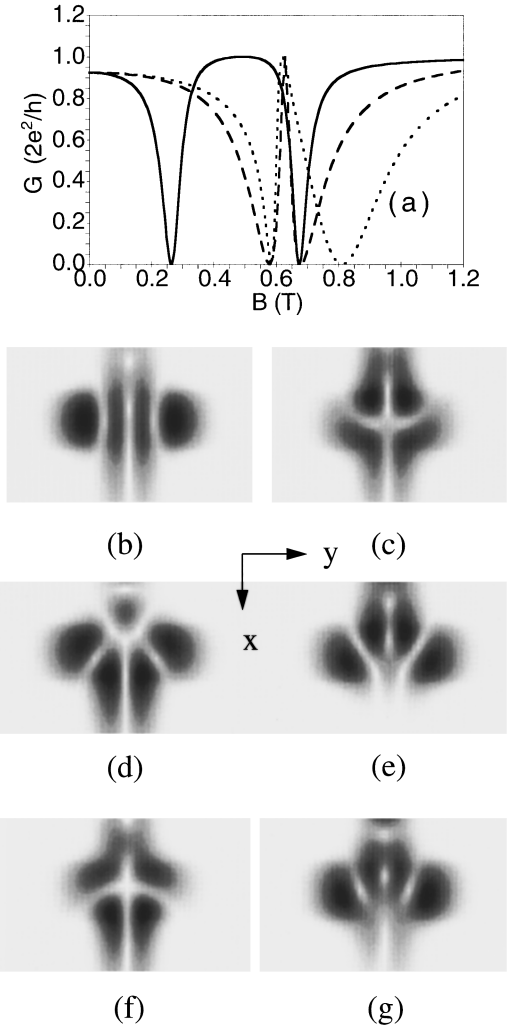

FIG. 5. (a) Conductance G vs B. The solid, dashed, and dotted curves correspond to $\omega_w/\omega_s=3.0$, 2.91, and 2.85, respectively. Note that two conductance minima occur in each curve. (b) In panels (b)–(g) the wave functions corresponding to these minima are plotted vs x and y with darker shading corresponding to higher amplitude. Panels (b) and (c) correspond to the first and second minima, respectively, for $\omega_w/\omega_s=3.0$; (d) and (e) correspond to $\omega_w/\omega_s=2.91$ and (f) and (g) to $\omega_w/\omega_s=2.85$.

occurring below the first propagating mode of the quantum wires, and a four-lobed excited state having the same odd symmetry of the state we see here.

In the curve for $\omega_w/\omega_s=3.0$, the two minima have a relatively large spacing in B. When $\omega_w/\omega_s=2.91$, the minima are quite close to each other, with the lower minimum occuring at a higher value of B, while the second one remains fixed. In fact, this is as close to each other as the minima get and they never merge for any value of ω_w/ω_s. This is a situation akin to an anticrossing from band structure theory. The wave functions for these two minima are shown in Figs. 5(d) and 5(e). These wave functions are virtual mirror images of each other and appear to be *hybrids* of the stub-confined and intersection-confined states shown in the previous two panels.

For $\omega_w/\omega_s=2.85$, the second minimum occurs at $B=0.8$ T a somewhat higher value of B than the previous two cases, while the first minimum occurs at $B=0.57$ T. The wave function corresponding to the first minimum of this curve is shown in Fig. 5(f). It is virtually a mirror reflection of the intersection-confined wave function shown in Fig. 5(c). The wave function for the second minimum in this case is shown in Fig. 5(g) and again has the hybrid form.

As is evident from our results, the relative positions of the two minima depend quite sensitively on ω_w/ω_s. It should be pointed out that, when ω_w/ω_s is increased 3.05, the lower conductance minimum no longer occurs leaving only the intersection-confined state at approximately the same position as it is for $\omega_w/\omega_s=3.0$. On the other hand, if ω_w/ω_s is decreased further below 2.85, the position of the lower minimum, which now corresponds to the intersection-confined state, occurs at lower and lower values of B, but it shifts less significantly than the second minimum which occurs at increasingly higher B values. That the intersection-confined state is less sensitive to changes in ω_w/ω_s is not surprising, since its presence should not depend too strongly on stub length. On the other hand, the reason why there is a shift at all in its position, when ω_w/ω_s is changed, is because while we are changing the stub length, we are also changing the confinement at the corners as well in our model.

IV. EXPERIMENTAL EVIDENCE FOR QUASIBOUND STATES

In this section, we present experimental results which lend support to our theoretical analysis and provide evidence for the presence of quasibound states in a DEST device and the appearance of new transmission minima under the influence of a magnetic field applied perpendicular to the device plane. Some preliminary results and details of sample fabrication and experimental measurement technique have been reported earlier.[14] The DEST device was fabricated using Schottky gates to define device geometry from a high-mobility ($\mu=110$ m^2/V$_s$ at 4.2 K) and low-electron-density ($n=3.1\times10^{15}$ m^{-2}) $Al_xGa_{1-x}As/GaAs$ modulation-doped (Si) heterostructure grown by molecular beam epitaxy and is shown in the inset of Fig. 6. The Fermi energy of the 2DEG was measured to be $E_F=8.50$ meV. The lithographic dimensions of the device were $a=b=2500$ Å, $c=8500$ Å, and $l=1500$ Å, respectively, l being the length of the connecting wires. Figure 6 shows the conductance G of the device in the absence of magnetic field measured as a function of gate voltage V_g at 70 mK. This temperature is a small fraction of E_F to be considered essentially zero. As V_g is made more negative, the device dimensions a, b, and c all decrease at the same time due to depletion. From measurements of the quantized conductance plateaus of a single quantum wire with lithographic width the same as that of the DEST wires, it was found that at $V_g=-500$ mV the Fermi level lies just below the bottom of the second ($n=1$) wire subband, and the corresponding wire width is 400 Å, so that for V_g (-500 mV) one could say that transport is in the fundamental mode of the connecting quantum wires and only the lowest ($n=0$) wire subband is occupied. Assuming the depletion at the stub edges is the same as that at the wire edges as the gate voltage is decreased, a rough estimate of the DEST dimensions at $V_g=-500$ mV could be obtained: $a=b=400$ Å, $c=6400$ Å. Though the estimate is rough, we can safely expect several DEST subbands to be occupied. Since the Fermi level is the same across the device and the Fermi energy does not change with V_g, a decrease in V_g accompanied by corresponding reduction of device dimensions means a decrease in the effective wire width and stub length as derived from the definition of classical turning points and given by Eq. (7). One could then say that the effective wire and stub confining frequencies increase as the gate voltage is made more negative. Since the depletion at the gate edges ($\simeq 2.9$ Å/mV) is the same for the wires and the stub, a change in V_g over a small range brings about little relative change in the stub length. However, for the wires, because of the much shorter dimension, the relative change in the wire width is quite important as V_g is swept. Considering the V_g range between -500 mV and pinch-off, one could then possibly consider

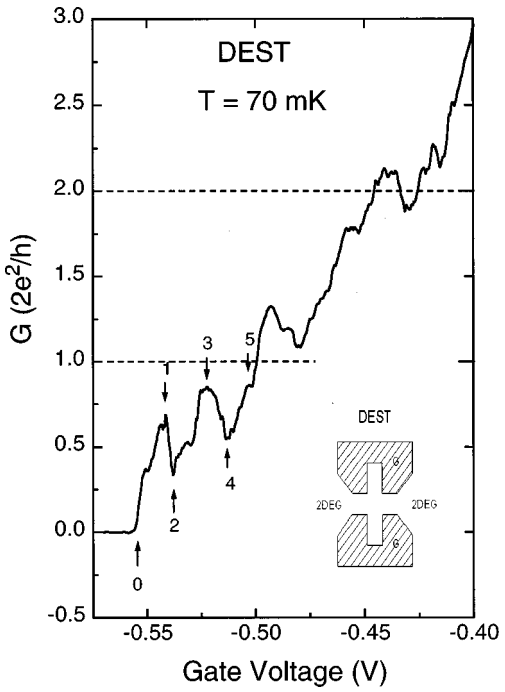

FIG. 6. Conductance G as function of gate voltage V_g for a nominally symmetric DEST at 70 mK. The numbers accompanied by arrows give stub subband indices. The inset shows a schematic drawing of the DEST geometry as defined by lithography. The hatched areas (G) represent Schottky gates.

the stub confining frequency ω_s to stay practically constant, while the wire confining frequency ω_w to increase rapidly with decreasing V_g. In Fig. 6, therefore, decreasing V_g would mean increasing the ratio ω_w/ω_s. It would also mean sweeping the Fermi level down across the stub subband levels given by ω_s. In Fig. 6, the conductance G shows two prominent minima and three maxima for V_g less than -500 mV. The observed minima can be attributed to an even-even coupling between the $n=0$ state in the wire and the $n=$even quasibound states in the stubbed cavity or DEST, as the Fermi level sweeps down the stub energy level structure. This analysis is in line with the theoretical prediction of the previous section and the observed minima can be considered as an experimental support of the theoretical analysis illustrated in Fig. 2(a). Note that in the present device geometry as V_g changes, the stub width changes as well. The observed minima are thus expected to be much broader than the theoretically predicted ones for a constant stub width. Moreover, the stub shape may also depend somewhat on the gate voltage. The shallowness of the minima can be attributed to asymmetry and/or defects,[18] while values of the maxima less than $2e^2/h$ can be attributed to backscattering at the wire entrance and/or impurities. For V_g larger than -500 mV, transport in both the wire and in the stub is multimode since one expects $a \sim b$. The resulting enhanced mixing between different modes will result in a more irregular G curve and may cause the regular oscillations observed below $V_g=-500$ mV to be gradually washed out as seen in Fig. 6. Based on the above analysis, we could index (n) the minima and maxima of Fig. 6. The indexing is shown by arrows. Using the known value of E_F and the above indexing, we get, for $V_g=-500$ mV, $\hbar\omega_w=5.67$ meV, and $\hbar\omega_s=1.030$ meV, giving $\omega_w/\omega_s=5.50$. This value is close to that used to generate Fig. 4(a). Note also that at this gate voltage $a=b=400$ Å. Figure 7 shows how the conductance maximum (index 5) of the DEST at $V_g=-500$ mV, changes under the influence of a magnetic field applied perpendicular to the plane of the device. We have added to Fig. 7, for comparison purposes, the theoretical curves of Fig. 4(a) which correspond to $b=400$ Å. As the field is increased, experimental G decreases and goes through a pronounced dip which corresponds to a transmission minimum. The minimum in G occurs at $B=0.29$ T, a value that is not strong enough to produce edge states. The experimentally observed minimum follows remarkably well the B dependence predicted by theory and may be understood in terms of the formation of a new quasibound state due to even-odd coupling induced by a weak magnetic field as discussed above. The shallowness of the observed dip may be due to an asymmetry of the experimental DEST as illustrated by the theoretical curves THA20 and THA40, respectively. The fabrication of a perfectly symmetric DEST is a matter of chance and cannot be *a priori* guaranteed. Given that the experimental curve is somewhat noisy in comparison to the smooth theoretical ones, the presence of disorder quite likely is playing a role as well.[18]

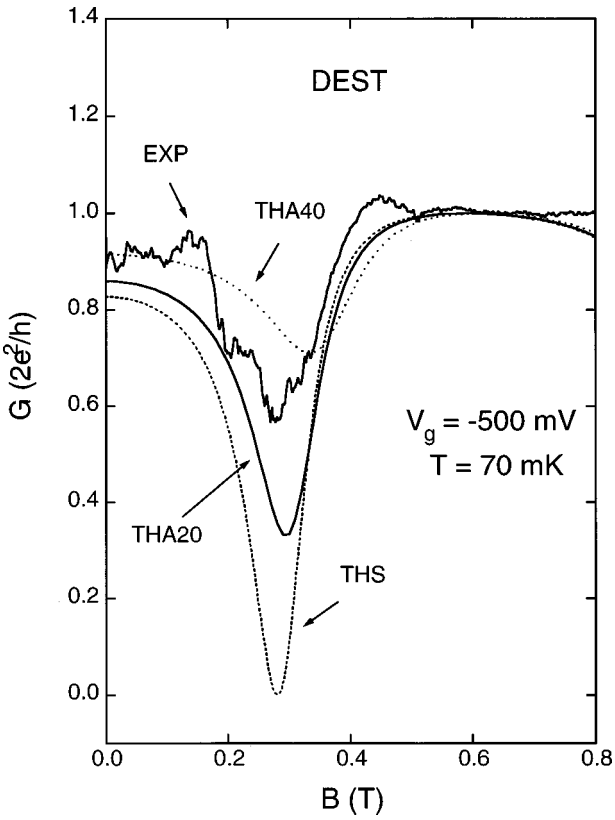

FIG. 7. Conductance G as function of magnetic field B applied perpendicular to device plane for the DEST shown in Fig. 6 at fixed $V_g=-500$ mV and 70 mK. The theoretical curves THS, THA20, and THA40 are reproduced from Fig. 4(a). THS : symmetric DEST; THA20: with offset 20 Å; THA40: with offset 40 Å. See text for details.

V. CONCLUSIONS

We have calculated the conductance for stubbed electron waveguides defined by a parabolic potential. In the absence of a magnetic field we find a *periodic* conductance output as the stubbed cavity is made longer, which is consistent with previous theoretical work done assuming infinite square well potentials. The conductance minima or *antiresonances* correspond to quasibound states in the stubbed regions. When the two parabolas representing the wire and stub confining potentials are displaced with respect to each other, the symmetry of the wave functions, with respect to the center of the wire, is broken and *new* quasibound states occur in the intersection regions. The same holds when the two parabolas are not displaced but a *weak* magnetic field B is present because the field too breaks this symmetry thus allowing states in the cavity and wire, that were previously orthogonal, to couple. The appearance of these quasibound states is heralded by one or more dips in the conductance as a function of magnetic field. We emphasize that these dips occur in short and long stubs, i.e, whether there are just a few or many stub subbands occupied for electrons incident at the Fermi energy. Such dips have been observed experimentally in electron waveguides with stubbed cavities.[14]

We have also investigated more sophisticated models for the confinement potentials, in particular models in which the transition between the quantum wire and stub regions is made gradually instead of abruptly as well as combinations of square well and parabolic confinement. We find that for the most part the results are qualitatively similar to those of the simple double parabolic model shown here. Importantly,

most quasibound states that occur when the transition in confinement is not abrupt, tend to be variations of the hybrid type discussed in the context of Fig. 5. In addition, we find that it is much more difficult to get the conductance minima at the low values of B considered here when all potentials are defined by infinite square-well confinement. Unless there is some rounding of the potentials, as one expects in real devices, the energy level spacing is too large to permit it.

Finally, in closing we note that the structures we have studied here can be thought of as ''simple'' quantum dots in the sense that relatively few nodes are apparent in the quasibound wave functions (four for the example in Fig. 5). The situation that is most typically studied in experiment and theory with regards to quantum dots is one in which the linear dimensions of the cavity are much larger than the width of the connecting wires (see, for example, Refs. 19 and 20 and references therein), so that the enclosed wave function can have hundreds of nodes. In these large cavities, ''scarring'' of resonant wave functions[19,20] has been observed, such that their amplitude is maximized along periodic classical trajectories.[21] These ''scarred'' features in these large open structures may result from a more complicated variation of the hybridization effect we have discussed here.

ACKNOWLEDGMENTS

The work of R.A. and P.V. was supported by NSERC Grant No. OGP0121756.

[1] For review articles on the subject see, C. W. J. Beenaker and H. van Houten, Solid State Phys. **44**, 1 (1991); S. E. Ulloa, A. MacKinnon, E. Castaño, and G. Kirczenow, in *Handbook on Semiconductors*, edited by P.T. Landsberg (Elsevier, Amsterdam, 1992), Vol. 1.

[2] F. M. Peeters, Superlattices Microstruct. **6**, 217 (1989).

[3] R. L. Schult, H. W. Wyld, and D. G. Ravenhall, Phys. Rev. B **41**, 12 760 (1990).

[4] J. J. Palacios and C. Tejedor, Phys. Rev. B **48**, 5386 (1993).

[5] W. Porod, Z. Shao, and C. S. Lent, Appl. Phys. Lett. **61**, 1350 (1992).

[6] P. J. Price, Appl. Phys. Lett. **62**, 289 (1993).

[7] E. Tekman and P. F. Bagwell, Phys. Rev. B **48**, 2553 (1993).

[8] K.-F. Berggren and Z.-L. Ji, Phys. Rev. B **43**, 4760 (1991).

[9] M. Leng and C. S. Lent, Phys. Rev. Lett. **71**, 137 (1993).

[10] A. B. Fowler, US Patent No. 4, 550,330 (29 October 1985); F. Sols, M. Macucci, U. Ravaioli, and K. Hess, Appl. Phys. Lett. **54**, 350 (1989); S. Datta, Superlattices Microstruct. **6**, 83 (1989).

[11] P. Debray, R. Akis, P. Vasilopoulos, and J. Blanchet, Appl. Phys. Lett. **66**, 3137 (1995).

[12] H. Wu, D. W. L. Sprung, J. Martorell, and S. Klarsfeld, Phys. Rev. B **44**, 6351 (1991).

[13] A. Kumar, S. E. Laux, and F. Stern, Appl. Phys. Lett. **54**, 1270 (1989).

[14] P. Debray, J. Blanchet, R. Akis, P. Vasilopoulos, and J. Nagle, in *21st International Symposium on Compound Semiconductors, San Diego, 1994*, edited by Herb Goronkin and Umesh Mishra, IOP Conf. Proc. No. 141 (Institute of Physics, and Physical Society, London, 1995), p. 835.

[15] T. Usuki, M. Saito, M. Takatsu, R. A. Kiehl, and N. Yokoyama, Phys. Rev. B **52**, 8244 (1995).

[16] R. Akis, P. Vasilopoulos, and P. Debray, Phys. Rev. B **52**, 2805 (1995).

[17] Z.-L. Ji and K.-F. Berggren, Phys. Rev. B **45**, 6652 (1992).

[18] R. Sordan and K. Nikolic, Phys. Rev. B **52**, 9007 (1995).

[19] R. Akis, D. K. Ferry, and J. P. Bird, Phys. Rev. B **54**, 17 705 (1996).

[20] R. Akis, D. K. Ferry, and J. P. Bird, Phys. Rev. Lett. **79**, 123 (1997).

[21] E. J. Heller, Phys. Rev. Lett. **16**, 1515 (1984).